The microkinetics of ammonia synthesis: the effect of surface coverage on apparent activation energy and reaction order

Ryusei Morimoto[1,†], *Takaya Ogawa*[2,†,*]

[1]*Undergraduate school of chemical science and technology, Faculty of Engineering, Kyoto University, Yoshida-Honmachi, Sakyo-ku, Kyoto 606-8501, Kyoto 606-8501, Japan*

E-mail address: morimoto.ryusei.86c@st.kyoto-u.ac.jp (R. M.)

[2]*Department of Socio-Environmental Energy Science, Graduate School of Energy Science, Kyoto University, Yoshida-Honmachi, Sakyo-ku, Kyoto Sakyo-ku, Kyoto 606-8501, Japan*

**Corresponding author. E-mail address: ogawa.takaya.8s@kyoto-u.ac.jp (T. O.)*

Abstract

We investigated the effect of coverage on the experimental results using Ru and Ru+K for ammonia synthesis at 0.1 MPa and 380~460℃. Especially for Ru+K, the reaction order changed significantly with temperature, and the rate-limiting step was also affected by temperature. The apparent activation energy decreased as the gas flow rate decreased, even when the total pressure was the same. We showed through experimental techniques that even relatively small changes in experimental conditions on a laboratory scale can change the coverage and have a non-negligible effect on the reaction order and apparent activation energy.

1. Introduction

Ammonia is an essential compound for human society as a raw material for artificial fertilizers. Its production is mainly synthesized in large-scale plants at a rate of 150 to 180 million tons per year, increasing by 2.3% per year [1]. Ammonia is also attracting attention as a renewable energy carrier since it can be synthesized from hydrogen obtained by water electrolysis using surplus electricity from solar and wind power generation [1, 2]. While hydrogen needs to be lowered to about -240°C to liquefy at 1 MPa, ammonia easily liquefies at room temperature at 1 MPa, thus liquefied ammonia has a higher energy density and is a superior energy carrier.

The amount of carbon dioxide emitted by industrial ammonia synthesis is equivalent to 1.4 % of total human emissions [3]. In the Haber-Bosch process, a typical method for industrial ammonia synthesis, Fe-based catalysts have been used for more than 100 years, and the addition of alkali metals enhances their activity [4]. In industrial processes, iron-based catalysts synthesize ammonia at 400-600°C and 100-300 atm [2, 4]. These severe conditions are due to the very high binding energy of the N_2 molecule (945 kJ mol^{-1}). Under these conditions, the cost of equipment such as a reactor becomes very expensive. Therefore, synthesis plants become massive and centralized to produce ammonia more cheaply and in large quantities for benefits of scales [5].

Ru-based catalysts, the next generation of ammonia synthesis catalysts, are less susceptible to ammonia poisoning and more active than Fe-based catalysts [4, 6]. In a volcano plot based on the adsorption energy of nitrogen molecules versus the reaction rate of ammonia synthesis, Ru is one of the best metals for ammonia synthesis [7]. On the other hand, Ru-based catalysts are more sensitive to hydrogen partial pressure than Fe-based catalysts and are more susceptible to hydrogen poisoning; the hydrogen order of Ru-based catalysts is often negative, while that of Fe-based catalysts is positive [8, 9]. However, Ru-based catalysts, which have

attracted much attention in recent years, are highly active and durable under surprisingly mild conditions on a laboratory scale by suppressing hydrogen poisoning of Ru [10-17]. These excellent Ru-based catalysts are expected to be applied to ammonia synthesis plants that are compact and inexpensive to construct and maintain [2, 18, 19]. This inexpensive small plant will enable locally produced and consumed ammonia synthesis, reducing transportation costs and helping to become self-sufficient in resources. In addition, highly distributed renewable energy can be efficiently used for small-scale ammonia synthesis in rural areas [20].

Reaction conditions in these large and small-scale plants are very different, and conditions at the laboratory scale are very different from those in industrial production. For example, flow rates, pressures, and temperatures vary, and catalyst activity is affected accordingly. The percentage of active sites on the catalyst surface occupied by the reacting molecules, i. e., coverage, is used as an indicator of such effects during the reaction. Coverage and elementary reactions on heterogeneous catalyst surfaces have been studied using chemisorption and electron diffraction in ultra-high vacuum, steady-state isotope transient kinetic analysis (SSITKA), and neutron diffraction (ND) measurements [21-25]. Fitting using the least-squares method has also been used to analyze and calculate the elementary reactions on the surface without direct observation [26, 27]. Such coverage depends on temperature and pressure, and even under the same conditions, it varies from catalyst to catalyst.

Today, the apparent activation energy and the reaction order are used as indicators of catalyst activity for Ru- and Fe-based catalysts. Both of them are affected by the coverage in the equation [28]. Therefore, they are affected by the reaction conditions because the coverage varies with the reaction conditions. In Fe-based catalysts with alkali metal additions, coverage and reaction order are temperature dependent [29]. First-principles calculations of the energy on the catalyst surface for Ru-based catalysts have also shown that the coverage and the reaction order are affected by temperature [30]. Understanding the effect of coverage on catalyst activity is critical to understanding elementary reactions on catalyst surfaces and creating better catalysts. Nevertheless, many current studies on lab scale compare catalysts measured under very different conditions.

However, no previous studies have experimentally evaluated how significant changes in coverage affect the apparent activation energy and reaction order at temperatures such as 400°C, where ammonia synthesis is generally carried out using Ru-based catalysts. Therefore, in this study, the equilibrium constants of each elementary reaction were obtained by fitting the experimental results of ammonia synthesis using Ru and Ru+K, and the coverage was derived from these values to investigate the effect of coverage on the apparent activation energy and the order of the reaction under various conditions. Two reaction models based on gas molecular kinetics were compared to select a more accurate reaction model to obtain more detailed coverage. The magnitude of the coverage effect on the apparent activation energy and the reaction order of Ru-based catalysts as a function of experimental conditions at the laboratory scale and the method for analyzing this effect was experimentally demonstrated.

2. Theoretical background and experimental method

2.1 Effect of surface coverage on apparent activation energy and reaction order.

The reactions on the catalyst surface are assumed to be based on the Langmuir-Hinshelwood mechanism, and the following reaction steps are assumed [31]. The * represents the active sites on the catalyst surface.

$$N_2 + * \rightleftarrows N_2 * \quad (1)$$

$$H_2 + 2* \rightleftarrows 2H* \quad (2)$$

$$N_2* + * \rightleftarrows 2N* \quad (3)$$

$$N* + H* \rightleftarrows NH* + * \quad (4)$$

$$NH* + H* \rightleftarrows NH_2* + * \quad (5)$$

$$NH_2* + H* \rightleftarrows NH_3* + * \quad (6)$$

$$NH_3* \rightleftarrows NH_3 + * \quad (7)$$

If the percentage of active sites on the surface of a given adsorbed species i, i.e., the coverage ratio, is denoted as θ_i then the fraction of empty sites used in the reaction, θ_V, is defined as follows.

$$\theta_V = 1 - \theta_{N_2} - \theta_H - \theta_N - \theta_{NH} - \theta_{NH_2} - \theta_{NH_3} \quad (8)$$

Assuming that the reverse reaction holds for all reactions and that Step 3 is the rate-limiting reaction, we can assume from the steady-state approximation that all other reactions reach equilibrium promptly. θ_V can be expressed using partial pressures and equilibrium constants as follows.

$$\theta_V = \frac{1}{1 + K_1 P_{N_2} + \sqrt{K_2 P_{H_2}} + \frac{P_{NH_3}}{K_2 K_4 K_5 K_6 K_7 P_{H_2}\sqrt{K_2 P_{H_2}}} + \frac{P_{NH_3}}{K_2 K_5 K_6 K_7 P_{H_2}} + \frac{P_{NH_3}}{K_6 K_7 \sqrt{K_2 P_{H_2}}} + \frac{P_{NH_3}}{K_7}} \quad (9)$$

Note that K_i is the equilibrium constant at step i, and k_i is the rate constant for the forward reaction in step i, k_{-j} is the rate constant for the reverse reaction in step j, and P_i is the partial pressure of reactant gas molecule i. Similarly, when step 3 is the rate-limiting step, if the forward reaction rate is r_+ and the reverse reaction rate of the is r_-, the overall reaction rate is shown below.

$$r = r_+ - r_- = k_3 \theta_{N_2} \theta_V - k_{-3} {\theta_N}^2 = k_3 K_1 P_{N_2} {\theta_V}^2 - k_{-3} \left(\frac{P_{NH_3}}{K_2 K_4 K_5 K_6 K_7 P_{H_2}\sqrt{K_2 P_{H_2}}} \right)^2 {\theta_V}^2 \quad (10)$$

Substituting Eq. 9 into Eq. 10, a model equation for the reaction rate considering the reverse reaction on the surface was derived, and this equation was used for fitting. For steps 4-7, the equations for the reaction rate and θ_V were derived (SI). A model that assumes that the reverse reaction in the rate-limiting step is negligible and that the ammonia adsorption reaction is also negligible was used for comparison (SI).

The reaction order was derived from the coverage. Although the reaction order includes both the forward and reverse orders of reaction (SI), only the combined reaction order can be observed experimentally, and what is obtained is only the "apparent" order of the reaction. When Step 3 is rate-limiting, the order of the reaction is

$$r = r_+ - r_- = k_3 \theta_{N_2} \theta_V - k_{-3} {\theta_N}^2 = k {P_{N_2}}^{\alpha} {P_{H_2}}^{\beta} {P_{NH_3}}^{\gamma} \quad (11)$$

α is the order of nitrogen, β is the order of hydrogen, and γ is the order of ammonia. Hence the order of hydrogen is

$$\beta = \frac{\partial \ln(r)}{\partial \ln(P_{H_2})} = \frac{\partial \ln(k_3 K_1 P_{N_2} {\theta_V}^2 - k_{-3} \left(\frac{P_{NH_3}}{K_2 K_4 K_5 K_6 K_7 P_{H_2}\sqrt{K_2 P_{H_2}}} \right)^2 {\theta_V}^2)}{\partial \ln(P_{H_2})} = \frac{3}{\frac{r_+}{r_-} - 1} + \frac{\partial \ln {\theta_V}^2}{\partial \ln P_{H_2}} \quad (12)$$

The order of hydrogen β was calculated in the same way for Steps 4-7 (SI). The ${}^{app}E_a$ is expressed as follows using the activation energy for the forward reaction $\overrightarrow{E_a}$ and the activation energy of the reverse reaction $\overleftarrow{E_a}$ Boltzmann's constant k_B and temperature T.

$${}^{app}E_a = -\frac{\partial(\ln r)}{\partial(1/k_B T)} = -\frac{\partial(\ln k_3 \theta_{N_2} \theta_V - k_{-3} {\theta_N}^2)}{\partial(1/k_B T)} = \overrightarrow{E_a} + \overleftarrow{E_a} - \frac{\partial(\ln \theta_{N_2} + \ln \theta_V + 2 \ln \theta_N + \ln \frac{r_+ - r_-}{r_+ r_-})}{\partial(1/k_B T)} \quad (13)$$

In the equilibrium state, the following equation is obtained.

$$\left.\frac{\theta_{\mathrm{i}}}{P_{\mathrm{i}}\theta^{*}}\right|_{\mathrm{Eq}} = \mathrm{K_{ads}} = e^{-\frac{\Delta G_{ads}}{k_B T}} \quad (14)$$

K_{ads} is the adsorption equilibrium constant, and ΔG_{ads} is the change in Gibbs free energy due to adsorption of gas molecule i. Eq. 12 and 13 show that the reaction order and $^{app}E_a$ are affected by the coverage. Eq. 14 shows that the coverage is affected by temperature. These equations are used in the following discussion.

2.3 Catalyst preparation. Ru powder (< 0.3 μm, 95% >) was purchased from Tokuriki Honten Co. K/Ru was prepared using KNO_3 aqueous solution (KNO_3; 99.9%, Fujifilm Wako Pure Chemical) so that the molar ratio of K to Ru was 1:1. K/Ru was held in a vacuum at 200˚C for 4 hours to evaporate water and NO_2 completely.

2.4 Characterization. The specific surface area was measured from the adsorption equilibrium of nitrogen at -196˚C using the Brunauer-Emmett-Teller (BET) method on an instrument (Tristar II Plus, micromeritics) after treatment of all samples in a vacuum at 200˚C for 2 hours**.** In addition, powder X-ray structure analysis (pXRD) was performed using the Cu Kα line (λ= 0.15417nm, 40 kV, 30mA).

2.5 Ammonia synthesis. The catalyst activity was measured in a stainless-steel tube reactor CSTR, using 0.05 g of Ru and 0.01 g of Ru+K, placed on quartz wool. All feed gases were high purity (99.9999%), N_2, H_2, and Ar. The gases were filtered to remove oxygen and water before being fed to the catalyst. Before the reaction, all samples were subjected to $N_2 + 3H_2$ at 0.1 MPa and raised to the target temperature at 200 ˚C h^{-1} . Apparent activation energies were derived based on the Arrhenius equation (see eq. 12), with Ru measured at 380~460°C and Ru+K at 380~440˚C. The reaction order was obtained based on $r = kP_{N_2}{}^{\alpha}P_{H_2}{}^{\beta}P_{NH_3}{}^{\gamma}$ (see eq. 11). The gas flow rates (N_2, H_2, Ar ml min^{-1}) were as follows. (20, 60, 0), (15, 45, 0), (10, 30, 0), (5,15, 0) for order of ammonia measurements, (5, 54, 1), (5, 42, 13), (5, 36, 19), (5, 30, 25), (5, 24, 31) for order of hydrogen measurements, (27, 24, 9), (22, 24, 14), (15, 24, 21), (10, 24, 26), (6, 24, 30) for order of nitrogen measurements. All ammonia syntheses were performed at 0.1 MPa. Synthesized ammonia was trapped in a 5 mM H_2SO_4 solution, and the concentration of NH_4^+ in the solution was measured by ion chromatography (Eco IC, metrohm). NH_3 effluents for all reactions were below 30% of equilibrium of NH_3 reaction.

2.6 Kinetic analysis. K_i, k_i, and the rate-limiting step were obtained by fitting the reaction order measurement results to a modeled reaction rate equation (see eq. 10)**.** Fitting was performed using experimental data and minimizing the following objective function SSE (sum of squared errors), i.e., the method of least squares.

$$SSE = \sum_{k=1}^{N} \left(\mathrm{r_{model}} - \mathrm{r_{exp}}\right)^2 \quad (15)$$

N is the total number of data used for fitting, and r_{model} and r_{exp} are the calculated and experimental values of the reaction rate, respectively. r_{model} is a function according to P_{H2}, P_{N2}, and P_{NH3} with k_i, K_i as constants (see eq. 10), k_i and K_i were obtained from fitting. K_i was constrained to be $1 \leq K_i\ (i = 1, 2, 3), K_j \leq 1\ (j = 4, 5, 6, 7)$, based on density functional theory (DFT) calculations in the work of Banisalman et al [32]. Constrained to be $K \geq 1$ is that the Gibbs energy of the reactant is equal to or less than the Gibbs energy of the product in the reaction, and $K \leq 1$ means that the Gibbs energy of the reactant is the same as or greater than the Gibbs energy of the product in the reaction. The reaction with the coefficient of determination R^2 closest to 1 was selected as the rate-limiting step. When the $\overline{r_{exp}}$ is the average of r_{exp}, the coefficient of determination is defined as follows, and the R^2 value is used as an index of the correlation between the modeled reaction rate and the experimental data.

$$R^2 = 1 - \frac{\sum_{k=1}^{N}\left(\mathrm{r_{model}} - \mathrm{r_{exp}}\right)^2}{\sum_{j=1}^{N}\left(\mathrm{r_{exp}} - \overline{\mathrm{r_{exp}}}\right)^2} \quad (16)$$

Results & discussion.

3.1 Catalysis Characterization. Surface area values from BET measurements, ammonia synthesis and $^{app}E_a$ under certain conditions are shown in Table 1. Ru was 4.4 m^2 g^{-1} and Ru+K was 4.7 m^2 g^{-1} by BET specific surface area measurement, which were almost the same. The $^{app}E_a$ were 118 kJ mol^{-1} for Ru and 111 kJ mol^{-1} for Ru+K. The purchased Ru powder has almost no impurities, and there is no potassium-derived peak in the XRD results of Ru + K, indicating that potassium is adsorbed as nanoparticles (Figure 1).

Tabel 1. Comparison of the catalysis.

catalyst	Surface area (m^2 g^{-1})	NH_3 formation (μmol g^{-1} h^{-1})	^{app}Ea (kJ mol^{-1})
Ru powder	4.4	2435	118
Ru + K	4.7	4488	111

i) Reaction conditions: flow rate 60 mL min^{-1} (H_2/N_2 = 3), 0.1 MPa, temperature 460˚C.

ii) $^{app}E_a$ is the apparent activation energy calculated from Arrhenius plots of the reaction rate in the temperature range of 380-460˚C for Ru, 380-440˚C for Ru+K, flow rate 60 mL min^{-1}, under 0.1MPa .

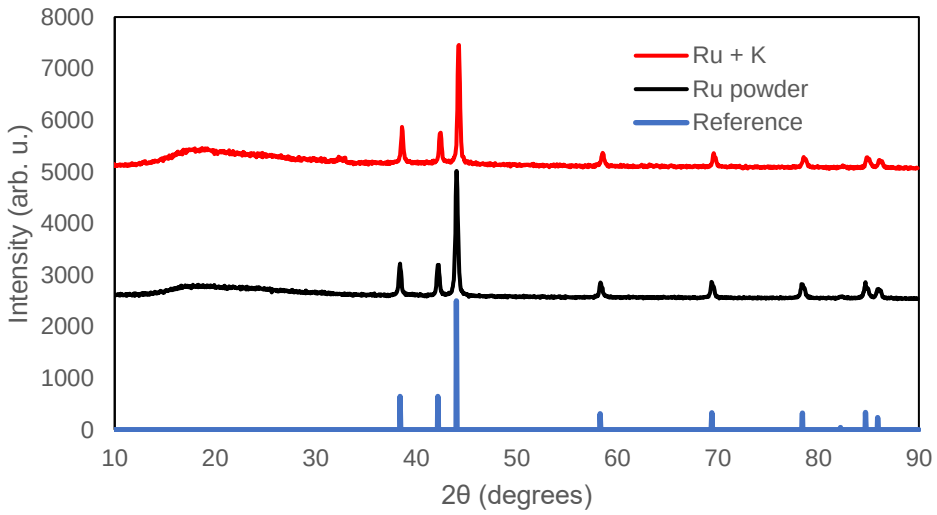

Figure 1 XRD patterns of Ru and Ru+K.

3.2 Surface coverage and reaction order.

3.2.1 Experimental results of reaction order. As shown in Section 2.1, the formula $^{app}E_a$ and the reaction order are affected by the coverage**.** In addition, the coverage is known to be temperature dependent (see eq. 14), and the reaction order varies with temperature. To demonstrate this experimentally on Ru catalysts, orders of reaction were measured at 380~460˚C. The results are shown in Figure 2. In the case of Ru, the order of H_2 was always about 1, and the order of N_2 was about -1 regardless of temperature. The order of NH_3 is negative at high temperatures and approaches zero at lower temperatures. On the other hand, for Ru+K, the order of NH_3, like Ru, tends to approach 0 as the temperature decreases, but the order of H_2, unlike Ru, becomes more negative as the temperature decreases. The order of the reaction shows different dependence on the catalyst.

3.2.2 Fitiing results using experimental data.

The rate-limiting step at each temperature was investigated by performing least-squares fitting (see eq. 15)

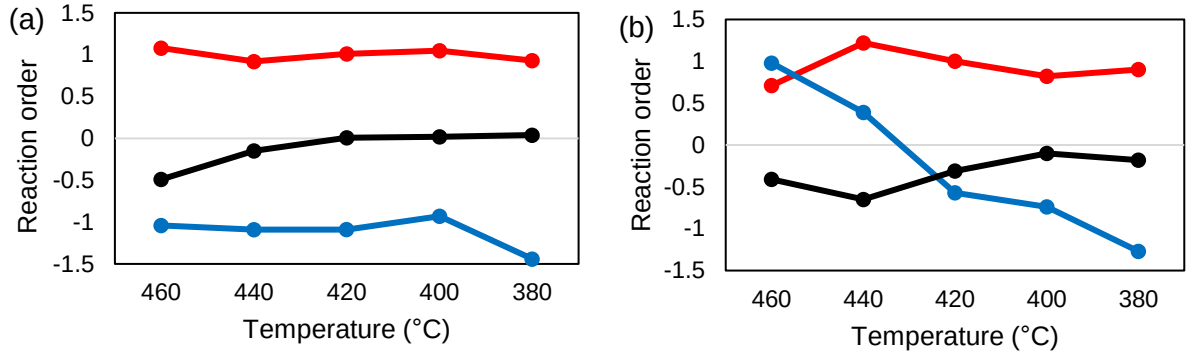

Figure 2. Temperature dependence of reaction order for (a) Ru, (b) Ru+K, total flow rate; 60mL min^{-1} . Red is order of N_2, blue is order of H_2, and black is order of NH_3.

to the model equation for the reaction rate. Before fitting the rate-limiting step at each temperature, the measured reaction order at 440˚C (Figure 2) was used to select a reaction model that more accurately described the experimental results and compared according to two models: a model that ignores the ammonia adsorption reaction and the reverse reaction in the rate-limiting step (Model I) and a model that considers the ammonia adsorption reaction and the reverse reaction in the rate-limiting step (Model II). The fitted results for Model I using Ru's experimental results are shown in Figure 3(i), and those for Model II are shown in Figure 3(ii). Comparing step 3 in Figure 3(i) and Figure 3(ii), R^2 is almost unchanged at 0.999 for both models, and the R^2 value for each model does not change much. Similarly, the R^2 values for steps 4, 5, and 6 did not change significantly. This trend is because the reverse reaction in step 3 can be ignored, which is the rate-limiting step, and the effect of the ammonia adsorption reaction on the coverage is limited. Figure 4 shows the results of the same experiment for Ru+K. As in Figure 3, the fitting results for the model without considering the reverse reaction (Model I) are shown in Figure 4 (i), and the fitting results for the model with the reverse reaction (Model II) are shown in Figure 4 (ii). The closest value of R^2 to 1 for each model is step 6, indicating that the rate-limiting step is step 6. Comparing Figure 4 (i) and (ii) for step 6, the R^2 value was 0.712 for the model I and 0.917 for model II. Model II had a larger R^2 value than Model I. Therefore, these results indicate that the model that considers the reverse reaction and the ammonia adsorption reaction can formulate the reaction rate more accurately.

Step 7, which was not considered in the model I, had an R^2 of 0.882 as shown in Figure 4 (ii). The fitting to the model equation assuming that the ammonia adsorption reaction in Step 7 is rate-limiting had not been examined in the previous study [25]. Therefore, the results of previous studies were fitted to the modeled reaction rate equations used in this study (SI).

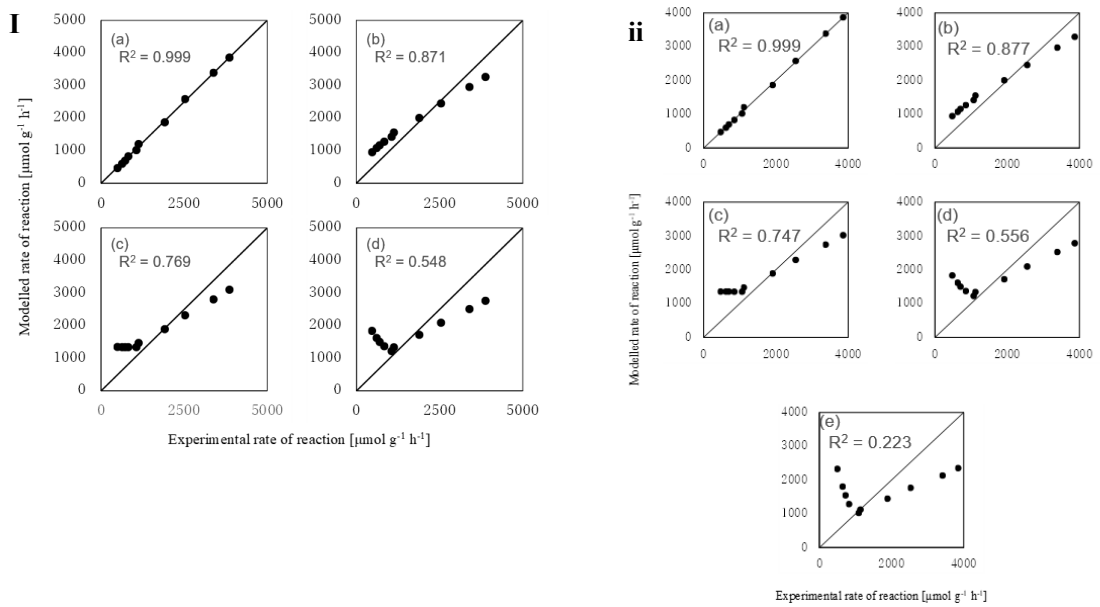

Figure 3. Best fitting results for reaction rates at 440°C over Ru powder; (i) not considering about ammonia adsorption reverse reaction (Model I), (ii) considering about ammonia adsorption reverse reaction (Model II) with respect to the rate equations derived with the rate-limiting step assumed to be (a) step 3 [N_2(ad) → 2N(ad)], (b) step 4 [N(ad) + H(ad) → NH(ad)], (c) step 5 [NH(ad) + H(ad) → NH_2(ad)], (d) step 6 [NH_2(ad) + H(ad) → NH_3(ad)], (e) step7 [NH_{23}(ad) + H(ad) → NH_3(ad)].

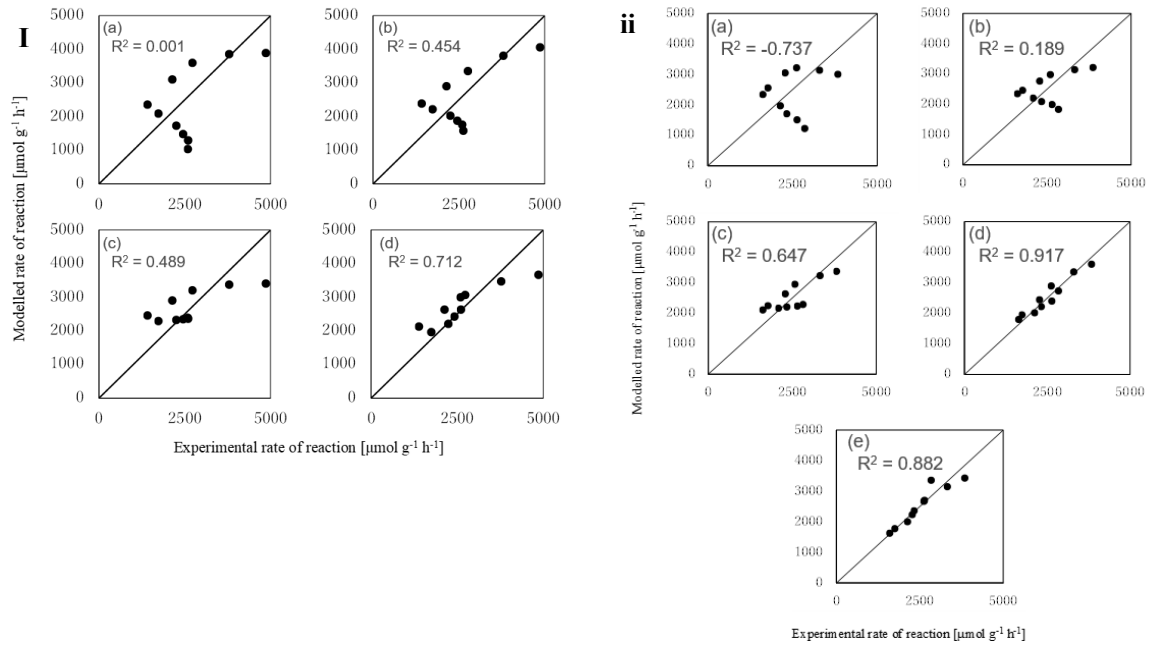

Figure4. Best fitting results for reaction rates at 440°C over Ru + K; (i) not considering about ammonia adsorption reverse reaction (Model I), (ii) considering about ammonia adsorption reverse reaction (Model II) with respect to the rate equations derived with the rate-limiting step assumed to be (a) step 3 [N_2(ad) → 2N(ad)], (b) step 4 [N(ad) + H(ad) → NH(ad)], (c) step 5 [NH(ad) + H(ad) → NH_2(ad)], (d) step 6 [NH_2(ad) + H(ad) → NH_3(ad)], (e) step7 [NH_{23}(ad) + H(ad) → NH_3(ad)]

In order to understand the cause of the temperature dependence of the reaction order difference between Ru and Ru+K (Fig. 2), we fitted a model (Model II) that considers the reverse reaction and the ammonia adsorption reaction at temperatures other than 440°C. Table 2 shows the coefficients of determination for the experimental

values of the reaction order measurement at 460~380˚C. The coefficients of determination for step 3 of Ru, R^2 are all ≥ 0.98, and the correlation between the modeled reaction rate and the experimental values is very strong. The Ru values of step 7, 6, 5, 4, and 3 gradually approached 1 for all temperatures. Therefore, it can be said that the rate-limiting step for Ru remained unchanged at step 3 even when the temperature was changed. For Ru+K, the R^2 value was closest to 1 at step 6 at 460˚C and 440˚C, step 4 at 420˚C, and step 3 at 400˚C and 380˚C, respectively. Therefore, the rate-limiting step was step 6 at 460˚C and 440˚C, step 5 at 420˚C, and step 3 at 400°C and 380˚C. Figure 2 and Table 2 show that as the reaction order changes with temperature, the rate-limiting step also changes with temperature.

Table 2. Coefficient determination of step 3~7 for Ru and Ru+K at 380~460°C.

	Ru					Ru + K				
Temperature (°C)	Step 3	Step 4	Step 5	Step 6	Step 7	Step 3	Step 4	Step 5	Step 6	Step 7
460	0.989	0.931	0.701	0.626	0.236	-0.737	0.189	0.647	0.917	0.882
440	0.999	0.877	0.747	0.556	0.223	0.001	0.454	0.703	0.858	0.688
420	0.997	0.81	0.689	0.528	0.252	0.905	0.924	0.868	0.682	0.308
400	0.996	0.781	0.559	0.509	0.25	0.981	0.924	0.836	0.628	0.265
380	0.984	0.777	0.668	0.478	0.252	0.999	0.849	0.741	0.491	0.23

To investigate the effect of the temperature dependence of the coverage (eq. 14) of each adsorbed species on the temperature dependence of the reaction order (Fig 2), the coverage at 380~460˚C when (N_2, H_2, Ar mL min^{-1}) = (5, 36, 19) was calculated. The results for (N_2, H_2, Ar mL min^{-1}) = (5, 54, 1) and (5, 24, 31) are shown in SI. θ_N, θ_V, and θ_{N2} tend to increase with increasing temperature. θ_H was also affected by temperature, but not as significantly. The rate-limiting step for Ru does not change with temperature, as shown in Table 2, so the abundance ratios of other adsorbed species (θ_V:θ_{N2}:θ_H) at each temperature are almost unchanged, except for θ_N. In the case of Ru+K (Figure 4), θ_N is smaller at lower temperatures as in the case of Ru. However, the temperature dependence of the other adsorbed species is significantly different from that of Ru. The ratio of adsorbed species (θ_V:θ_{N2}:θ_H:θ_{NH2}:θ_N) also varies significantly with temperature. Based on Table 2, the abundance ratios of adsorbed species at 460 and 440˚C, where the rate-limiting step is step 6, are close, and those at 400 and 380˚C, where the rate-limiting step is step 3, are close. Thus, the factor affecting the overall reaction, i.e., coverage, changes as the rate-limiting step changes.

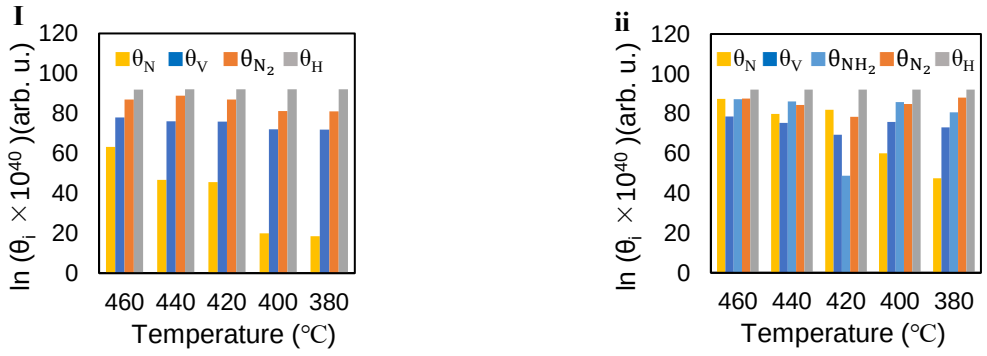

Figure 5. Temperature dependence of coverage for various species over Ru (i) and Ru+K (ii), gas flow rate (N_2, H_2, Ar) = (5, 36, 19).

3.2.3 Calculated reaction order from In both of the catalysts, the R^2 values of the steps with the highest R^2 values at each temperature are greater than 0.85 (Table 2). However, the fact that the R^2 value is close to 1 indicates a strong correlation between the model equation of the reaction rate and the experimental results. On the other hand, it does not complement the plausibility of each parameter, such as equilibrium constants and the surface coverage in the model equation. Therefore, to confirm the accuracy of the equilibrium constants and coverage ratios, the hydrogen orders were calculated using the arguments in Equation 12 to see how close they are to the experimental results. The results are shown in Figure 6. In the case of Ru, the reaction order values calculated from the coverage tended to become more negative as the temperature decreased but did not perfectly reproduce the experimental values. In the case of Ru+K, the reaction order values calculated from the coverage showed a tendency to become more negative with decreasing temperature. The calculated values from the coverage are very close to the experimental values, which guarantees the coverage accuracy calculated from the fittings. As shown in Table 2, Ru has the closest R^2 value to 1 at step R^2 than Ru+K for all temperatures. However, Figure 6 shows that the order of hydrogen calculated by the coverage derived from the fitting results is closer to the experimental value for Ru+K. Therefore, when the R^2 value is closer to 1, not only there is a strong correlation between the model equation values and the experimental values, but the K_i, k_i obtained from the fitting and the coverage factor θ_i calculated from them are also obtained at an appreciable level.

The experimental coverage on the catalyst surface obtained using SSITKA was compared with the coverage values calculated using our method in Supporting Information.

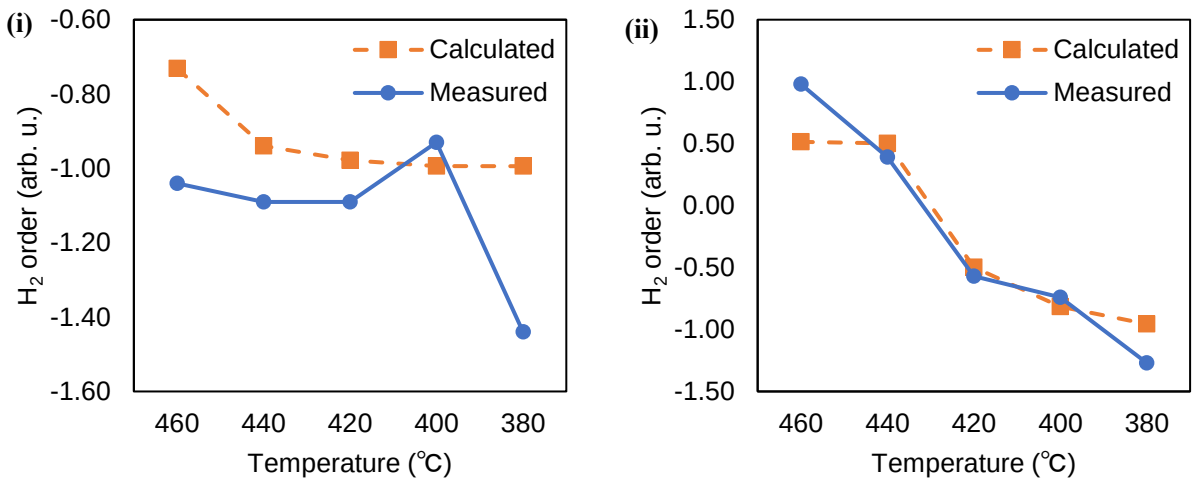

Figure 6. Calculated and measured order of hydrogen for Ru (i) and Ru+K (ii).

3.3 Apparent activation energy.

3.3.1 Experimental result of apparent activation energy. To investigate the effect of coverage on $^{app}E_a$, $^{app}E_a$ was measured by varying the reactant gas flow rate. Figure 7 shows that the lower the gas flow rate, the smaller the $^{app}E_a$. Coverage significantly affects $^{app}E_a$ with the very small change in reaction conditions. The lower the flow rate, the higher the ammonia concentration (vol%). This tendency is consistent with previous studies [30]. When overall flow rates are lower, the number of adsorbed species derived from the feed molecules decreases and the relative concentration of product ammonia increases, increasing the ammonia partial pressure and facilitating the adsorption of ammonia-derived adsorbed species on the catalyst surface and increasing the coverage (Figure 5, Table 2). Therefore, the lower the flow rate, the lower the $^{app}E_a$, because the increased

product-derived coverage makes the reverse reaction more likely to occur, and because ammonia synthesis is an exothermic reaction, the reverse reaction is more likely to occur at higher temperatures (Figure 7).

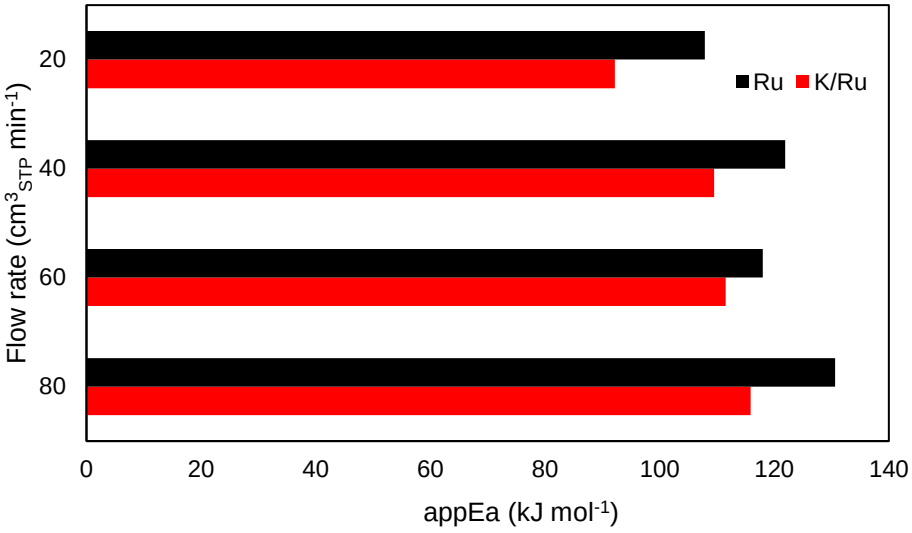

Figure 7. Flow dependence of ^{app}Ea over Ru.

3.3.2 Coverage effect on $^{app}E_a$. To further illustrate the relationship between coverage and $^{app}E_a$, the relationship between $^{app}E_a$ and coverage for each adsorbed species is shown in Figure 8, based on the results for Ru shown in Figure 2 and Figure 5. On the other hand, $^{app}E_a$ increases as θ_H increases. This indicates that hydrogen poisoning of Ru increases $^{app}E_a$, while an increase of θ_V and θ_{N2} on the surface decreases $^{app}E_a$. In Figure 5, it was difficult to see the temperature variation of θ_H, but Figure 8(ii) shows clearly that θH is smaller at higher temperatures. In addition, it was experimentally shown that $^{app}E_a$ is affected by the coverage as well as the reaction order for Ru-based catalysts.

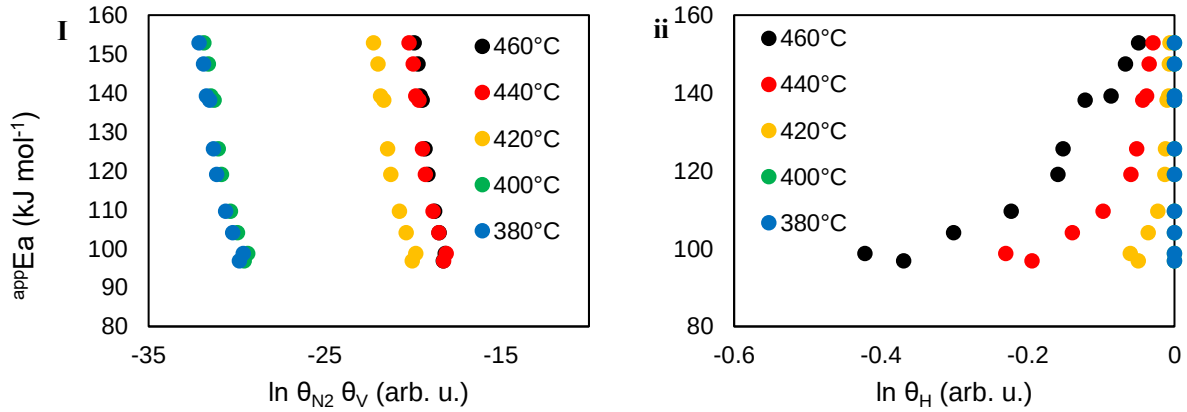

Figure 8. Coverage dependence of $^{app}E_a$.

Model II is also important for the discussion of coverage, since it allows an accurate evaluation of θ_{NHx} (x = 0, 1, 2, 3) by considering the reverse reaction in the rate-limiting step and the ammonia adsorption reaction. For example, if step 3 is the rate-limiting step, then $\theta_{NHx} = 0$ in Model I. The effect of these adsorbed species on $^{app}E_a$ and the reaction order cannot be understood. On the other hand, Model II allows us to know the effect of

θ_{NHx} on $^{app}E_a$ and reaction order, and also allows us to describe a more accurate model when fitting the reaction rate to the model equation (see fig 3 and 4).

It can be added from Figure 2 and Figure 6 that these differences in models change the coverage and affect the experimental results. In the case of Ru, the reaction order calculated from the coverage is closer to the experimental value for the model that does not consider the reverse reaction (Model I), but there is not much difference except for the hydrogen order at 460˚C (Figure 9).

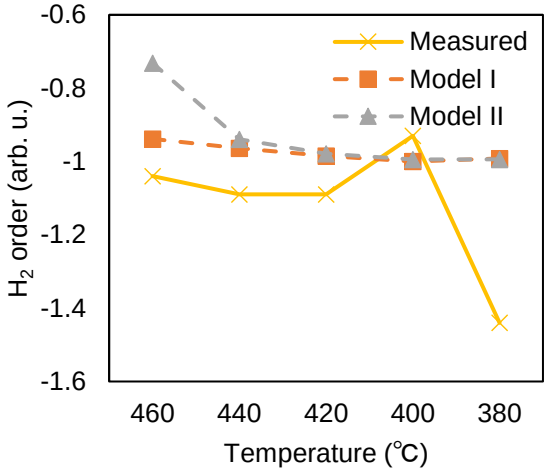

Figure 9. Calculated and measured order of hydrogen for Ru.

In the case of Ru+K, on the other hand, the model considering the reverse reaction was closer to the experimental value (SI). This is because the rate-limiting step in Ru is nitrogen dissociation which makes it difficult for the reverse reaction to occur. The rate-limiting step in Ru+K is NH_3* formation (step 6) at high temperatures, which makes the reverse reaction more likely to occur. There are also advantages of adopting a model that considers the reverse reaction in the rate-limiting step and ammonia adsorption reaction not only for Ru+K but also for Ru. As shown in Figure 10, the coverage calculated based on Model II (i, ii) shows a clear temperature dependence, i.e., the higher the temperature, the smaller the coverage. In contrast, Model I (iii) invert the results measured at 380°C and 400°C (ii). In other words, the accuracy of the fitting is better when the inverse reaction is taken into account, as it clearly shows the temperature dependence of the coverage. As shown in Figure 5, the calculated reaction order for Ru+K is relatively close to the experimental value, while for Ru the calculated value deviates from the experimental value, suggesting room for improvement in fitting.

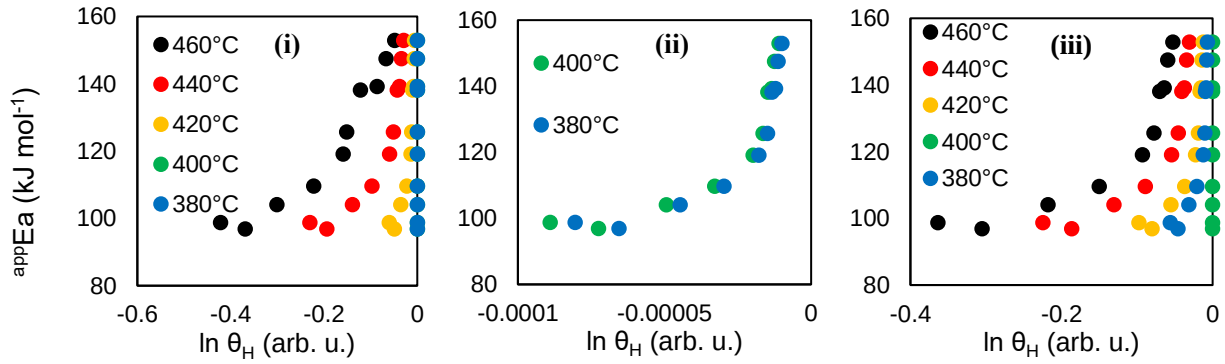

Figure 10. Coverage dependence of $^{app}E_a$.

Under the conditions generally employed for lab-scale ammonia synthesis rate measurements, coverage is

affected by partial pressure and temperature (Figure 5), and changes in coverage affect the reaction order and $^{app}E_a$ (Figures 6, 8). The fact that these experimental conditions affect $^{app}E_a$ and reaction order indicates that when comparing catalysts, those two indicators can be very different under the same conditions, or that there is a risk that performance can rapidly worsen by changing pressure or temperature for the same catalyst.

4. Conclusion

The surface coverage (and its partial pressure dependence) obtained from fittings on Ru-based catalysts was found to reproduce the experimental results. In particular, it was shown for the first time that the reaction order varies depending on the coverage not only for Fe-based catalysts but also for Ru-based catalysts, even within the range of reaction conditions commonly used in the literature. The $^{app}E_a$ is also affected by the coverage as well as the reaction order. When comparing the catalyst of interest with catalysts measured under different conditions and highlighting the differences, the differences in $^{app}E_a$ and reaction order might be small when measured under the same conditions. This suggests the risk that the performance of the catalyst of interest can change significantly with changes in conditions such as temperature, pressure, flow rate, and reactor volume. In addition, it was shown that the influence of coverage can be elucidated by analyzing the reaction kinetics of ammonia synthesis from a kinetic point of view without using experimental techniques such as chemisorption. On the other hand, the fittings used in the analysis are not perfect, and this method may replace other experimental methods for the evaluation of adsorbed species on catalyst surfaces in the future.

Acknowledgment

This research was supported by the Environment Research and Technology Development Fund (JPMEERF20192R02) of the Environmental Restoration and Conservation Agency of Japan.

Author Contributions

†R. M. and T. O. contributed equally to this work

References

[1] Morlanés, N et al. *Chem. Eng. J*. 2021, 408, 127310.

[2] Juangsa, F. B.; Irhamna, A. R.; Aziz, M. *Int J Hydrogen Energy*, 2021, 46, 14455-14477.

[3] MacFarlane, D. R.; Cherepanov, P. V.; Choi, J.; Suryanto, B. H. R.; Hodgetts, R. Y.; Bakker, J. M.; Ferrero Vallana, F. M.; Simonov, A. N. A Roadmap to the Ammonia Economy. *Joule*, 2020, 4 (6), 1186− 1205.

[4] Liu, H. *Chin. J. Catal*., 2014, 35(10), 1619-1640.

[5] Brown, D.E.; Edmons, T.; Joyner, R. W.; MaCarroll, J.J.; Tennison, S. R. *Catal Lett*, 2014, 144, 545-552.

[6] Rosowski, W.; Hormung, A.; Hinrichsen, O.; Herein, D.; Muhler, M.; Etrl, G. *Appl.Catal. A,* 1997, 151, 443

[7] Jacobsen, C. J. H.; Dahl, S.; Clausen, B. S.; Bahn, S.; Logadottir, A.; Nørskov, J. K. *J. Am. Chem. Soc*. 2001, 123, 8404−8405.

[8] Marakatti, V. S.; Gaigneaux, E. M. *ChemCatChem*, 2020, 12, 1-21.

[9] Aika, K.; Ozaki, A.; Hori, H. *J. Catal*. 1972, 27, 424

[10] Kitano, M.; Inoue, Y.; Yamazaki, Y.; Hayashi, F.; Kanbara, S.; Matsuishi, S.; Yokoyama, T.; Kim, S. W.; Hara, M.; Hosono, H. *Nat. Chem*. 2012, 4, 934.

[11] Tang, Y.; Kobayashi, Y.; Masuda, N.; Uchida, Y.; Okamoto, H.; Kageyama, T.; Hosokawa, S.; Loyer, F.; Mitsuhara, K.; Yamanaka, K.; Tamenori, Y.; Tassel, C.; Yamamoto, T.; Tanaka, T.; Kageyama. *Adv. Energ. Mater*. 2018, 8 (36), 1801772.

[12] Li, L.; Zhang, T.; Cai, J.; Cai, H.; Ni, J.; Lin, B.; Lin, J.; Wang, X.; Zheng, L.; Au, C. T.; Jiang, L. *J. Catal. 2020*, 389, 218−228

[13] Yamashita, H.; Broux, T.; Kobayashi, Y.; Takeiri, F.; Ubukata, H.; Zhu, T.; Hayward, M. A.; Fujii, K.; Yashima, M.; Shitara, K.; Kuwabara, A.; Murakami, T.; Kageyama, H. *J. Am. Chem. Soc*. 2018, 140 (36), 11170− 11173.

[14] Kitano, M.; Inoue, Y.; Ishikawa, H.; Yamagata, K.; Nakao, T.; Tada, T.; Matsuishi, S.; Yokoyama, T.; Hara, M.; Hosono, H. *Chem. Sci*. 2016, 7 (7), 4036−4043

[15] Ogawa, T.; Kobayashi, T.; Mizoguchi, H.; Kitano, M.; Abe, H.; Tada, Y.; Toda, Y.; Niwa, Y.; Hosono, H. *J. Phys. Chem. C*. 2018, 122 (19), 10468-10475.

[16] Zhang, X.; Liu, L.; Wu, A.; Zhu, J.; Si, R.; Guo, J.; Chen, R.; Jiang, Q.; Ju, X.; Feng, J.; Xiong, Z.; He, T.; Chen, P. *ACS Catal*. 2022, 12 (4), 2178−2190.

[17] Sato, K.; Miyahara, S.; Ogura, Y.; Tsujimaru, K.; Wada, Y.; Toriyama, T.; Yamamoto, T.; Matsumura, S.; Nagaoka, K. *ACS Sustain. Chem. Eng.* 2020, 8 (7), 2726−2734.

[18] Ventures, P. Nitrogen. 2018, 354, 1.

[19] Demirhan, C.D.; Tso, W.W.; Powell, J.B.; Pistikopoulos, E.N. *AIChE Journal*, 2019, 65 (7), e16498.

[20] Pepermans, G.; Driesen, J.; Haeseldonckx, D.; Belmans, R.; D'haeseleer, W. *Energy Pol,* 2005, 33, 787e98.

[21] Ledesma, C.; Yang, J.; Chen, D.; Holmen. *ACS Catal*. 2014, 4 (12), 4527−4547.

[22] Kammert, J et al. *J. Am. Chem. Soc*. 2020, 142, 7655.

[23] Etrl, G. *Critical Reviews in Solid State and Material Sciences.* 1982, 10 (4), 349.

[24] Nørskov, J. K.; Houmøller, A.; Johansson, P. K.; Lundqvist, B. I. *Phys. Rev. Lett*. 1981, 46, 257.

[25] Stoltze, P.; Nørskov, J. K. *Phys. Rev. Lett*. 1985, 55, 2502.

[26] Kobayashi, Y.; Kitano, M.; Kawamura, S.; Yokoyama, T.; Hosono, H. *Catal. Sci. Technol*. 2017, 7, 47.

[27] Siporin, S. E.; Davis, R. J. *J. Catal*. 2004, 225, 359-368.

[28] Lynggaard, H et al. *Progress in Surface Science*. 2004, 77, 71-137.

[29] Stoltze, P. *Phys Scr.* 1987, 36, 824-864.

[30] Hellman, A et al. *Surface Science.* 2009, 603, 1731.

[31] Langmuir, I. *Trans. Faraday Soc.* 1922, 17, 621–654.

[32] Banialman, M. J.; Kim, M.; Han, S. S. *ACS Catal*. 2022, 12, 1090-1097.